Prediction of molecular targets for zedoary turmeric oil in inhibiting proliferation and inducing apoptosis in non-small cell lung cancer

HUAIYONG LI[1*], LILI LIU[2*], QINGZHU YANG[2], YAO LI[2], YONGLI SONG[1], JING JIANG[1], ZHENZHONG WU[1], WEIWEI ZHANG[2] and BAISONG LOU[1]

[1]Department of Chemoradiotherapy, The First Hospital of Qiqihar, Qiqihar, Heilongjiang 161000, P.R. China; [2]Department of Life Science and Agroforestry, Qiqihar University, Qiqihar, Heilongjiang 161006, P.R. China

Received January 22, 2026; Accepted May 13, 2026

DOI: 10.3892/mmr.2026.13932

Abstract. In the present study, the inhibitory effects of zedoary turmeric oil (ZTO) on non-small cell lung cancer (NSCLC) were investigated using integrated network pharmacology, molecular docking and *in vitro* experiments. Treatment with 100 μg/ml ZTO in A549 cells and 50 μM ZTO in H1299 cells markedly reduced cell viability (assessed through an MTT assay), suppressed proliferation (assessed through colony formation/EdU assays) and increased apoptosis (assessed through flow cytometry). Network analysis identified 27 bioactive components (such as curcumadione and zedoradiol) and 96 shared targets with NSCLC. Core targets (including ESR1, EGFR, PIK3CA and PIK3CB) were found to be enriched in the EGFR/PI3K/Akt signaling pathway. Molecular docking demonstrated stable binding between the ZTO components and these targets. Furthermore, reverse transcription-quantitative PCR and western blotting revealed that ZTO downregulated ESR1 and EGFR expression ($P<0.05$). These findings suggested that ZTO suppressed NSCLC progression by modulating the EGFR/PI3K/Akt pathway, with its active components potentially targeting key oncogenic regulators. The present study therefore highlights the therapeutic potential of ZTO as a multi-target agent against NSCLC.

Correspondence to: Dr Baisong Lou, Department of Chemoradiotherapy, The First Hospital of Qiqihar, 30 Gongyuan Road, Longsha, Qiqihar, Heilongjiang 161000, P.R. China
E-mail: 13604521696@163.com

Professor Weiwei Zhang, Department of Life Science and Agroforestry, Qiqihar University, 42 Wenhua Street, Jianhua, Qiqihar, Heilongjiang 161006, P.R. China
E-mail: 02065@qqhru.edu.cn

*Contributed equally

Key words: network pharmacology, zedoary turmeric oil, non-small cell lung cancer, ESR1, EGFR

Introduction

Lung cancer exhibits the highest incidence and mortality rate worldwide, with ~85% of cases being histologically classified as non-small cell lung cancer (NSCLC), of which 55-60% are adenocarcinomas (1). The majority of early-stage patients with NSCLC remain undiagnosed due to the absence of clinical manifestations; when symptoms do occur, they primarily include cough and hemoptysis. The treatment for patients with locally advanced NSCLC primarily includes chemotherapy, immunotherapy, molecular targeted therapy and radiotherapy (2,3). Despite marked improvements in patient prognosis through advancements in targeted and immunotherapeutic approaches, the 5-year survival rate remains below 37% (4). These challenges underscore the need to develop innovative therapeutic strategies and identify effective chemotherapeutic agents to improve clinical outcomes.

Curcuma zedoaria Rosc. is a Traditional Chinese Medicine component previously recorded in 'Chinese Pharmacopeia' (5) amongst others (6). It is primarily cultivated in Guangxi and Zhejiang provinces and its rhizome, belonging to the *Curcuma* genus of the *Zingiberaceae* family, yields zedoary turmeric oil (ZTO), a volatile extract (7). ZTO has been shown to exhibit multifaceted antitumor properties against lung adenocarcinoma, including suppression of A549 cell proliferation (8), mitigation of chemotherapy-induced adverse effects (9) and enhancement of radiosensitivity in advanced patients with NSCLC (10). However, the clinical use of ZTO is hindered by its complex chemical composition and potential adverse reactions, such as respiratory system damage and allergic reactions (11-13), underscoring the imperative to isolate bioactive monomers. Network pharmacology, an emerging paradigm in systems biology, provides a robust framework to elucidate the multi-component, multi-target and multi-pathway synergy of Traditional Chinese Medicine (14). In the present study, network pharmacology was employed to identify the main bioactive components, therapeutic targets and associated signaling pathways of ZTO in NSCLC treatment. The core targets were further validated through molecular docking and *in vitro* cellular experiments, with the aim of delineating the pharmacodynamic basis of ZTO and optimizing its clinical utility.

Materials and methods

Key materials. Human NSCLC cell lines A549 (cat. no. CM-0016) and H1299 (cat. no. CM-0165) were purchased from Procell Life Science & Technology Co., Ltd. and cultured at 37˚C in 5% CO_2 in DMEM (Gibco; Thermo Fisher Scientific, Inc.) or RPMI-1640 (Gibco; Thermo Fisher Scientific, Inc.). ZTO injection (Zhejiang Tianrui Pharmaceutical Co., Ltd.; national medical product approval/lot no. H20064312; cat. no. 423020101), F12K medium (cat. no. 21127030; Thermo Fisher Scientific, Inc.), FBS (cat. no. C04001-500; Shanghai XP Biomed Ltd.) and trypsin (cat. no. PB180225; Procell Biotechnology Co., Ltd.) were used. The BeyoClick™ EdU Cell Proliferation Kit with AF488 (cat. no. C0071S; Beyotime Biotechnology), 4% paraformaldehyde (cat. no. P0099; Beyotime Biotechnology), Acridine Orange Staining Kit (cat. no. C0233S; Beyotime Biotechnology), Annexin V-FITC Apoptosis Detection Kit (cat. no. BA00101; Beijing Biosynthesis Biotechnology Co., Ltd.), TRIzol® Reagent (cat. no. 15596026CN; Invitrogen; Thermo Fisher Scientific, Inc.) and Reverse Transcription Kit and Real-Time Quantitative PCR Kit (cat. nos. AG0304-B and AH0104-B; Shandong Sparkjade Biotechnology Co., Ltd.) were used. Instruments used included the Spark™ 10M microplate reader (Tecan Group Ltd.), Z32HK high-speed refrigerated centrifuge (HERMLE Labortechnik GmbH) and Mastercycler® Realplex4 Real-Time PCR System (Eppendorf SE).

MTT assay. A549 cells and H1299 cells in the logarithmic growth phase were seeded into 96-well plates and cultured for 24 h. Subsequently, the A549 cells were treated with ZTO at final concentrations of 0, 100, 200, 300 and 400 μg/ml at 37˚C for 48 h and the H1299 cells were treated with ZTO at final concentrations of 0, 20, 40, 60, 80, 100, 120 and 140 μM at 37˚C for 48 h. After incubation, 10 μl MTT solution (0.5 μg/μl) was added to each well and incubated at 37˚C for 4 h. Subsequently, 150 μl DMSO was added to each well and allowed to stand for 10 min. The absorbance was measured at 490 nm using a multimode microplate reader.

Clonogenic survival assay. After A549 and H1299 cells were treated with 100 μg/ml and 50 μM ZTO for 48 h, A549 and H1299 cells were resuspended at a density of 100 cells/ml and 1 ml cell suspension was seeded into 12-well plates. Cells were cultured in a 37˚C, 5% CO_2 incubator for 7-10 days until ~50 cell colonies formed per well. The cultures were then terminated, washed twice with PBS and fixed with methanol at room temperature for 30 min. The cells were then stained with 0.1% crystal violet at room temperature for 1 h, gently rinsed under running water, air-dried and photographed. The number of colonies was quantified using ImageJ software (version 1.54k; National Institutes of Health). A colony was defined as a cluster of ≥50 cells; ImageJ counts were manually verified to ensure consistency with this definition.

EdU assay. A549 and H1299 cells were seeded in 6-well plates at a density of $5x10^5$ cells/ml (2 ml/well) and cultured for 12 h. A549 cells were then treated with 100 μg/ml ZTO and H1299 cells were treated with 50 μM ZTO for 48 h at 37˚C. Cell proliferation was assessed using the EdU Cell Proliferation Detection Kit (Beyotime Biotechnology), according to the manufacturer's instructions. The percentage of EdU-positive cells was calculated from five randomly selected images using ImageJ software (version 1.54k).

Wound-healing assay. The A549 and H1299 cells were cultured until they reached 80-90% confluence, after which, they were treated with 100 μg/ml and 50 μM ZTO for 48 h at 37˚C, respectively. Subsequently, the A549 and H1299 cells were scratched using a sterile 200-μl pipette tip. The detached cells were gently washed away with PBS, and serum-free medium was added. Wound closure was monitored and images were captured at 0, 6 and 24 h post-scratching. The migration rate was quantified by measuring the wound area at each time point using ImageJ software (version 1.54k).

Transwell migration assay. After A549 and H1299 cells were treated with 100 μg/ml and 50 μM ZTO for 48 h at 37˚C, respectively, they were trypsinized, resuspended in serum-free medium and adjusted to $1x10^5$ cells/ml. Then, a 300-μl cell suspension was added to the upper chamber of a Transwell insert (12-well plate; 8-μm pore size; Corning, Inc.), and 500 μl medium supplemented with 20% FBS was added to the lower chamber as a chemoattractant. After 24 h of incubation at 37˚C with 5% CO_2, the cells that migrated to the lower membrane surface were fixed with 4% paraformaldehyde for 0.5 h, stained with 0.1% crystal violet for 1 h at room temperature and rinsed with distilled water. The inserts were air-dried, mounted on glass slides with neutral resin, and images were captured under a light microscope (Olympus IX72; Olympus Corporation). Migrated cells were counted in five randomly selected fields per well using ImageJ software (version 1.54k).

Cell morphological analysis. A549 and H1299 cells were seeded onto glass coverslips in 6-well plates and cultured for 12 h. A549 cells were then treated with 100 μg/ml ZTO and H1299 cells were treated with 50 μM ZTO for 48 h. The culture medium was removed and the cells were washed twice with PBS. Then, cells were fixed with methanol for 30 min at room temperature. After two additional PBS washes, cells were stained with acridine orange for 5 min at room temperature in the dark, then rinsed three times with PBS to remove excess dye. The coverslips were carefully inverted onto microscope slides freshly coated with anti-fade mounting medium (applied 1-2 min before mounting) at room temperature and images were immediately captured using a laser scanning confocal microscope (LSM 880; Zeiss AG) with appropriate filter sets for acridine orange detection (excitation/emission: 488/525 nm).

Annexin V-FITC. After A549 and H1299 cells were treated with 100 μg/ml and 50 μM ZTO for 48 h, respectively, they were trypsinized (using EDTA-free trypsin), transferred to centrifuge tubes and pelleted by centrifugation at 1,000 x g for 5 min at 4˚C. The supernatant was discarded and cells were resuspended in PBS, then centrifuged (1,000 x g, 5 min, 4˚C). Cell pellets were stained with 5 μl Annexin V-FITC and 10 μl PI solution, followed by incubation at 37˚C in the dark for 30 min with gentle mixing. The cell suspensions were then filtered through a 400-mesh nylon sieve and analyzed using

a Cytomics FC500 Flow Cytometer (Beckman Coulter, Inc.) within 1 h. All samples were analyzed with CXP Software ver.2.3 (Beckman Coulter, Inc.). Apoptotic populations were quantified using Annexin V-FITC+/PI-(early apoptosis), Annexin V-FITC+/PI+ (late apoptosis/necrosis) and Annexin V-FITC-/PI-(viable cells).

Platforms, software and databases used for network pharmacology. Specific platforms, software and databases used for network pharmacology analysis are shown in Table I.

Target prediction of active constituents in ZTO. Primary chemical constituents of ZTO were systematically retrieved from the Traditional Chinese Medicine Systems Pharmacology database (TCMSP) and supplemented with evidence from the literature (7,11,12). The chemical structures of the identified compounds were analyzed using the PubChem database, while putative therapeutic targets were predicted using the Swiss Target Prediction database. Targets with a probability >0 were selected as the target proteins. Probability indicates the confidence level of the predicted interaction between the compound and the target.

Screening of ZTO targets for NSCLC. Potential therapeutic targets associated with NSCLC were identified by searching the Online Mendelian Inheritance in Man (OMIM) database, GeneCards database and Therapeutic Target Database (TTD) using the keyword 'non-small cell lung cancer'. The retrieved targets were combined and duplicate entries were eliminated. High-confidence targets were then prioritized based on relevance scores and functional annotations.

Construction of the ZTO-NSCLC compound-target network. Overlapping targets between ZTO active components and NSCLC were identified and the 'ZTO-NSCLC Compound-Target Network' was constructed using Cytoscape (version 3.10.1) (15). Node degree values were analyzed and the top five active components with the highest degree values were selected to visualize their pharmacological associations.

Construction of protein-protein interaction (PPI) network and screening of key targets. Standard targets of ZTO for lung cancer treatment were imported into the Search Tool for the Retrieval of Interacting Genes/Proteins (STRING) database (version 12.0), with the species limited to *Homo sapiens* and a confidence score threshold of >0.900. Disconnected nodes were excluded to generate the PPI network. Network topology analysis was conducted using Cytoscape (version 3.10.1) and the degree values of each target were calculated to identify hub genes.

Gene ontology (GO) and Kyoto encyclopedia of genes and genomes (KEGG) enrichment analysis. Overlapping target genes between ZTO and NSCLC were imported into the DAVID database for GO and KEGG pathway enrichment analysis. Visualization of the enrichment results, including bubble plots and bar charts, was performed using the Bioinformatics Online Analysis Platform (https://www.bioinformatics.com.cn/).

Molecular docking analysis. SDF files of the primary active components of ZTO were retrieved from the PubChem database, while the 3D structures of key target proteins were collected from the Protein Data Bank (PDB; https://www.rcsb.org/). The protein structures were optimized by removing water molecules using PyMOL (version 2.1.0; Schrödinger, Inc.), followed by hydrogenation and format conversion to PDBQT using AutoDock Tools (version 1.5.6; Molecular Graphics Laboratory, The Scripps Research Institute). Molecular docking was performed using the AutoDock Vina (version 2.0) module embedded in PyRx software (version 0.8; https://pyrx.sourceforge.io/) to calculate binding energies and generate output files.

Reverse-transcription quantitative PCR (RT-qPCR). After treatment with 100 μg/ml ZTO for 48 h, the mRNA expression levels of ESR1 and EGFR in A549 cells were analyzed using RT-qPCR. Total RNA was extracted and reverse-transcribed into cDNA using the ReverTra Ace™ qPCR RT Master Mix with gDNA Remover (Toyobo Co., Ltd.), as described by Zhang *et al* (16). qPCR was performed with TB Green Premix Ex Taq (Tli RNaseH Plus; cat. no. RR420L; Takara Bio, Inc.) by cycling at 95˚C for 2 min, followed by 40 cycles of 95˚C for 15 sec and 60˚C for 30 sec. All reactions were run in triplicate and relative gene expression was calculated using the $2^{-\Delta\Delta Cq}$ method (17). The primer sequences used, including that of the reference gene β-actin, are listed in Table II.

Western blotting. Whole-cell lysate was prepared using RIPA lysis buffer (cat. no. P0013B; Beyotime Biotechnology). The lysate was centrifuged at 13,000 x g at 4˚C for 15 min. The supernatant was collected and protein concentration was measured with a BCA protein assay kit (Beyotime Biotechnology). Equal amounts of protein (12 μg per lane) were loaded onto 10% SDS-PAGE gels, separated and then transferred to PVDF membranes. The membranes were blocked with BeyoFC™ Fc Receptor Blocking Solution (Human) (Beyotime Biotechnology) at room temperature for 15 min, then incubated overnight at 4˚C with primary antibodies against ESR1 (1:300; cat. no. WL00940; Shenyang Wanli Biotechnology Co., Ltd.) and EGFR (1:300; cat. no. CY5064; Shanghai Abways Biotechnology Co., Ltd.). Afterward, the membranes were incubated with IRDye® 800CW goat anti-rabbit IgG secondary antibody (1:15,000; cat. no. 926-32211; LICORbio) or IRDye® 800CW goat anti-mouse secondary antibody (1:15,000; cat. no. 926-32210; LICORbio) at room temperature for 1 h, then washed with 1X PBS-0.1% (v/v) Tween-20 (pH 7.4). The western blots were visualized using the Odyssey® Infrared imaging system (LI-COR Biosciences) and the bands were analyzed and normalized to mouse β-actin (1:5,000; cat. no. ab8227; Abcam). using ImageJ software.

Mycoplasma testing. A 2-3 day-old cell culture medium was used as the sample for *Mycoplasma* testing. A 30 μl PCR reaction was assembled by adding 15 μl TransDetect® PCR Mycoplasma SuperMix II (2x; TransGen Biotech Co., Ltd.), 2 μl Myco Primer Mix II, 8 μl MycoFree Water and 5 μl template in that order. Both a negative control (MycoFree Water) and a positive control (MycoPositive Control Template II) were included. The following program was then

Table I. Technical specifications: Platforms, software and databases.

Platforms, software or database	URL
Traditional Chinese Medicine Systems Pharmacology Analysis platform	http://tcmspw.com/index.php
Swiss Target Prediction	http://www.swisstargetprediction.ch/
PubChem database	https://pubchem.ncbi.nlm.nih.gov/
GeneCards database	http://www.genecards.org
Online Mendelian Inheritance in Man database	http://www.omim.org
Therapeutic Target Database	http://db.idrblad.net/ttd
Search Tool for the Retrieval of Interacting Genes/Proteins database	http://cn.string-db.org
DAVID database	https://david.ncifcrf.gov/
Research Collaboratory for Structural Bioinformatics Protein Data Bank	https://www.rcsb.org/
Bioinformatics Online Analysis Platform	https://www.bioinformatics.com.cn/

Table II. Primers used for reverse transcription-quantitative PCR.

Primer	Direction	Sequence (5'-3')
ESR1	Forward	GCTTACTGACCAACCTGGCAGA
	Reverse	GGATCTCTAGCCAGGCACATTC
EGFR	Forward	AACACCCTGGTCTGGAAGTAC
	Reverse	TCGTTGGACAGCCTTCAAGACC
β-actin	Forward	AGCGAGCATCCCCCAAAGTT
	Reverse	GGGCACGAAGGCTCATCATT

run: initial denaturation at 95˚C for 4 min; 35 cycles of 95˚C for 10 sec, 62˚C for 25 sec and 72˚C for 10 sec; final extension at 72˚C for 5 min. A total of 10 μl product was loaded on a 1.5% agarose gel. Following electrophoresis, the gel was stained with ethidium bromide and visualized under UV transillumination; a ~254 bp band indicated a positive result. The samples were compared with controls to determine *Mycoplasma* contamination.

Statistical analysis. Statistical analyses were performed using SPSS (version 25.0; IBM Corp.) and GraphPad Prism (version 8.0; Dotmatics) software. Intergroup differences were evaluated using unpaired Student's t-test. Data are expressed as the mean ± SD. $P<0.05$ was considered to indicate a statistically significant difference.

Results

ZTO inhibits proliferation of lung cancer A549 cells and H1299 cells. To investigate the effects of different concentrations of ZTO on the proliferation of human lung cancer cell lines A549 and H1299, the inhibitory effects were measured using an MTT assay. The results demonstrated that ZTO inhibited the proliferation of both cell lines in a concentration-dependent manner (Fig. 1A). The IC_{50} values were determined to be 96.73 μg/ml for A549 cells and 46.82 μM for H1299 cells. Therefore, ZTO concentrations of 100 μg/ml and 50 μM were selected for subsequent experiments. The colony-forming efficiency and percentage of EdU-positive cells in both A549 and H1299 cells were found to be significantly decreased compared with the control group (Fig. 1B and C).

ZTO inhibits the migration of lung cancer A549 and H1299 cells. Effects of ZTO on the migratory capacity of A549 and H1299 cells were evaluated by wound-healing and Transwell assays. Compared with the control group, the wound healing rate and number of migrated cells were markedly reduced in the ZTO-treated groups (Fig. 2). These results indicated that ZTO suppressed the migration of lung adenocarcinoma cells.

ZTO induces apoptosis in lung cancer A549 cells and H1299 cells. As shown in Fig. 3A, acridine orange staining revealed that untreated A549 and H1299 cells exhibited high density, intact cellular structure and nearly round nuclei. By contrast, ZTO-treated cells displayed marked morphological changes, including cell shrinkage, chromatin condensation in the nuclei and early apoptotic alterations. The Annexin V-FITC/PI dual staining results demonstrated that, compared with the control group, ZTO treatment significantly increased the early apoptosis rate of A549 and H1299 cells (Fig. 3B). These findings collectively indicated that ZTO promoted apoptosis in A549 cells.

Screening of ZTO components and target prediction results. Through the TCMSP database and supplementary literature review, >100 components from ZTO were identified. Based on preliminary experiments and screening criteria from the literature, 27 major active components of ZTO were identified (Table III). Subsequently, target prediction was performed for these active components. After entering the components into the database and applying filtering parameters (probability >0), 301 target genes were obtained for further analysis.

Network pharmacological analysis of ZTO-NSCLC interactions. Using 'non-small cell lung cancer' as the keyword, 156 targets were retrieved from the OMIM database, 1,317 targets (with relevance score >4 times the median value) from the

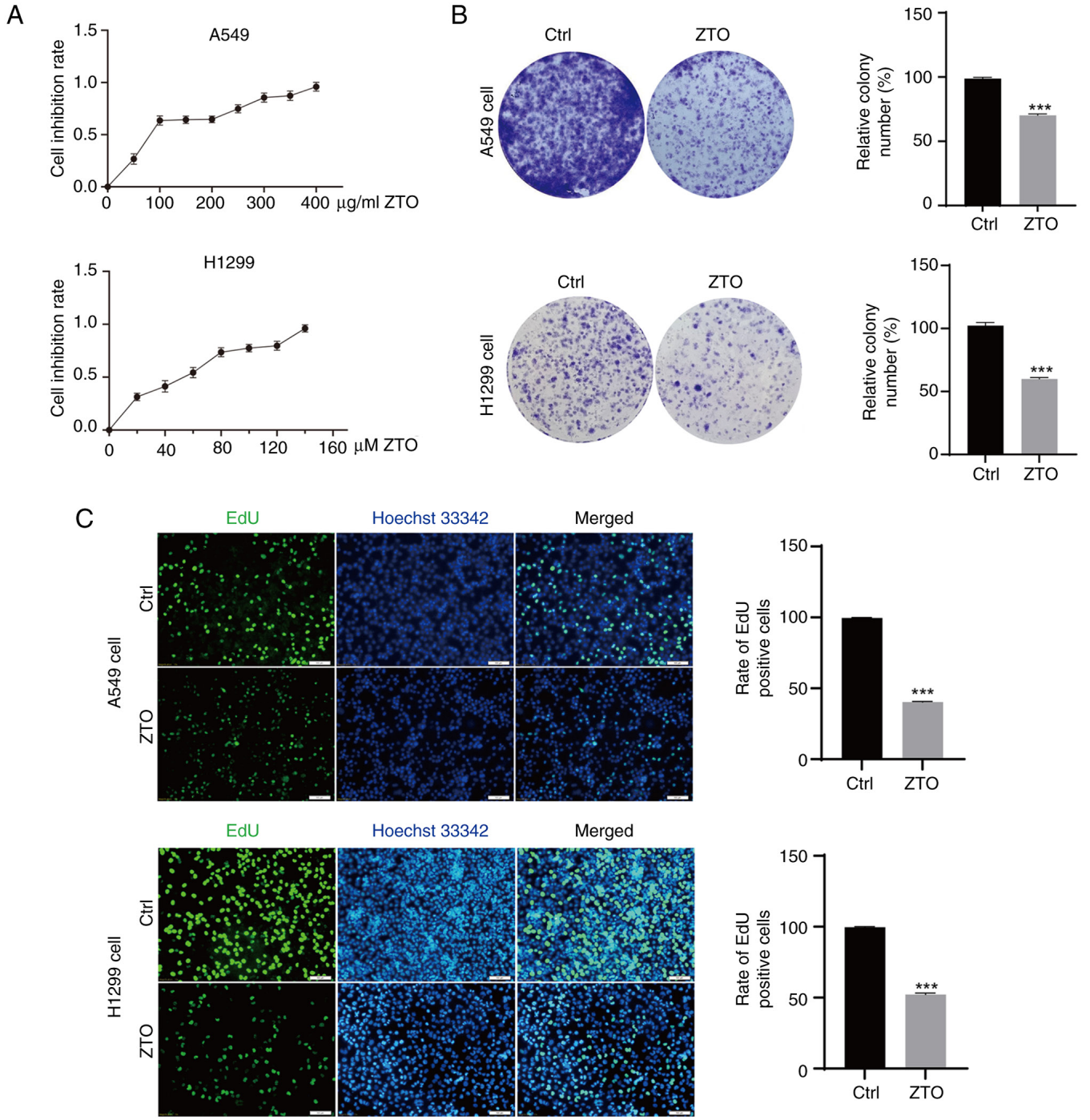

Figure 1. Inhibitory effect of ZTO on the proliferation of human lung cancer A549 cells. (A) MTT assay for detecting the proliferation inhibition rate of A549 cells and H1299 cells by ZTO. (B) Clone formation assay. (C) EdU method for detecting the proliferation of human lung cancer A549 cells and H1299 cells. Compared with the control group. Scale bar, 100 μm (original magnification, x100). ***P<0.001. ZTO, zedoary turmeric oil; Ctrl, control.

GeneCards database and 100 targets from the TTD database. After merging and deduplication, 1,483 NSCLC-associated targets were identified. A cross-analysis of 301 ZTO targets and 1,483 NSCLC targets identified 96 common drug-disease targets (Table SI). A ZTO-NSCLC compound-target interaction network diagram was then constructed (Fig. 4A), whereby the number of edges emitted by active compounds reflects their potential regulatory scope. The top five active compounds with the highest target connectivity were curcumenone, zedoarondiol, 13-hydroxygermacrone, neocurdione and curcumol, indicating their key roles in NSCLC intervention.

The 96 overlapping targets were further analyzed using the STRING database to build a PPI network (Fig. 4B), comprising 96 nodes and 202 edges. Visualization and topological analysis using Cytoscape (Fig. 4C and Table IV) revealed that node size and color intensity were associated with degree values. The top five core targets ranked by degree values were ESR1, EGFR, PIK3CA, PIK3CB and PTPN11, indicating their central roles in mediating the anti-NSCLC effects of ZTO.

GO and KEGG pathway enrichment analysis. GO functional enrichment analysis of the 96 overlapping targets

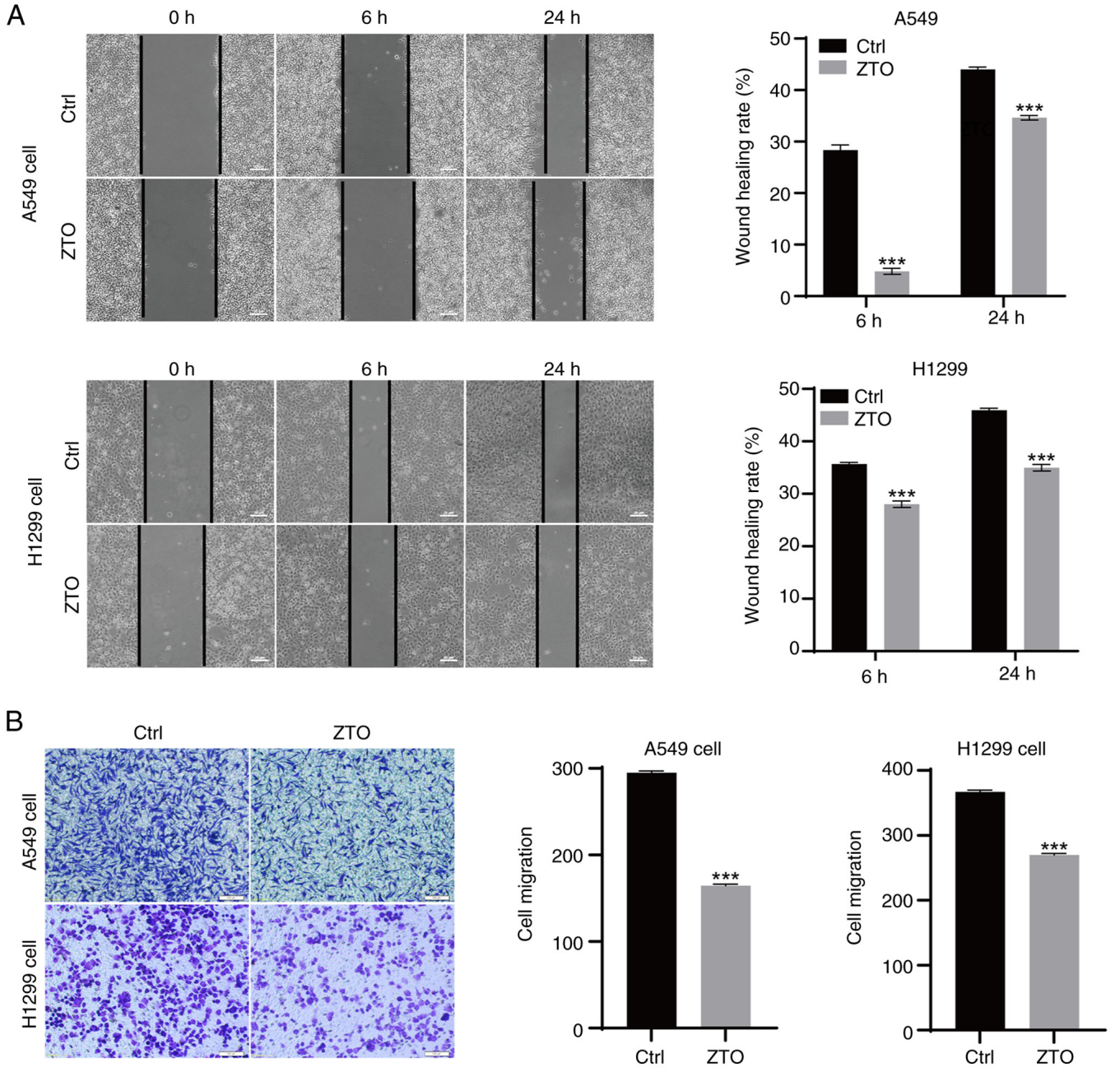

Figure 2. ZTO inhibits the migration of lung cancer A549 and H1299 cells. (A) A scratch wound healing assay was used to assess the migratory ability of A549 cells and H1299 cells. Scale bar, 25 μm (original magnification, x400). (B) A Transwell migration assay was used to evaluate the migratory capacity of A549 cells and H1299 cells (purple indicates crystal violet staining). Scale bar, 100 μm (original magnification, x100). ***P<0.001 compared with the control group. ZTO, zedoary turmeric oil; Ctrl, control.

was performed using the DAVID database, yielding 526 significant entries (Fig. 5A). These included 391 biological process terms primarily associated with 'Signal transduction', 'Phosphorylation' and 'Response to xenobiotic stimulus', 52 cellular component terms enriched in the 'Cytoplasm', 'Nucleus' and 'Membrane raft' as well as 83 molecular function terms mainly associated with 'Protein tyrosine kinase activity', 'Transcription coactivator binding' and 'Protein kinase binding'. KEGG pathway enrichment analysis identified 526 significant pathways (Fig. 5B), predominantly associated with 'EGFR tyrosine kinase inhibitor resistance', 'PI3K-Akt signaling pathway', 'Pathways in cancer', 'HIF-1 signaling pathway' and 'Proteoglycans in cancer'. These results suggested that ZTO exerted therapeutic effects on NSCLC through multi-target modulation of oncogenic signaling pathways and regulation of cellular proliferation.

Molecular docking validation. Molecular docking was performed to validate the interactions between the top five core components of ZTO (curcumenone, curcumadiol, 13-hydroxygermacrone, neocurdione and curcumol) and the key targets (ESR1, EGFR, PIK3CA, PIK3CB and PTPN11) identified for NSCLC treatment. The results demonstrated that the binding energies of all active components with the core targets were <-5.0 kcal/mol, indicating spontaneous and stable binding (Table V). The binding mode analyses, focusing on

Table III. Basic information of chemical composition of zedoary turmeric oil.

First author, year	PubChem no.	Chemical component	Simplified molecular input line entry system	(Refs.)
Zhong *et al*, 2025	CID14543198	Isoprocurcumenol	CC(=C1CC2C(CCC2(C)O)C(=C)CC1=O)C	(7)
	CID24836956	Neocurdione	CC1CCC=C(CC(=O)C(CC1=O)C(C)C)C	
	CID6441391	Curdione	CC1CCC=C(CC(=O)C(CC1=O)C(C)C)C	
	CID14240392	Curcumol	CC1CCC2C13CC(C(O3)(CC2=C)O)C(C)C	
	CID167812	Curcumenol	CC1CCC2C13CC(=C(C)C)C(O3)(C=C2C)O	
	CID10399139	Isocurcumenol	CC1CCC2C13CC(=C(C)C)C(O3)(CC2=C)O	
	CID3081930	Curzerenone	CC1=COC2=C1C(=O)C(C(C2)(C)=C)C(=C)C	
	CID6436348	Germacrone	CC1=CCC(=C(C)C)C(=O)CC(=CCC1)C	
	CID572766	Curzerene	CC1=COC2=C1CC(C(C2)(C)C=C)C(=C)C	
	CID6918391	β-Elemene	CC(=C)C1CCC(C(C1)C(=C)C)(C)C=C	
	CID6442617	Dehydrocurdione	CC1CCC=C(CC(=O)C(=C(C)C)CC1=O)C	
	CID24834047	Zedoarondiol	CC(=C1CC2C(CCC2(C)O)C(CC1=O)(C)O)C	
	CID6654	α-Pinene	CC1=CCC2CC1C2(C)C	
	CID6616	Camphene	CC1(C2CCC(C2)C1=C)C	
	CID6552009	Camphor	CC1(C2CCC1(C(C2)O)C)C	
	CID64685	Borneol	CC1(C2CCC1(C(C2)O)C)C	
Yang *et al*, 2022	CID91753231	Germacrone-4, 5-epoxide	CC1=CCCC2(C(O2)CC(=C(C)C)C(=O)C1)C	(12)
	CID12309452	γ-Elemene	CC(=C1CCC(C(C1)C(=C)C)(C)C=C)C	
	CID12309449	δ-Elemene	CC(C)C1=CC(C(CC1)(C)C=C)C(=C)C	
	CID10399140	13-Hydroxygermacrone	CC1=CCC(=C(C)CO)C(=O)CC(=CCC1)C	
	CID14191393	Curcumanolide A	CC1CCC(C12CC(=C(C)C)C(=O)O2)C(=C)C	
	CID5315469	Bisacumol	CC1=CC=C(C=C1)C(C)CC(C=C(C)C)O	
	CID10263440	Epiprocurcumenol	CC1=CC(=O)C(=C(C)C)CC2C1CCC2(C)O	
	CID636458	Furanodiene	CC1=CCC2=C(CC(=CCC1)C)OC=C2C	
	CID14543200	Neoprocurcumenol	CC1=C2CCC(C2CC(=C(C)C)C(=O)C1)(C)O	
Wu *et al*, 2022	CID91457	β-Eudesmol	CC12CCCC(=C)C1CC(CC2)C(C)(C)O	(11)
	CID153845	Curcumenone	CC(=C1CC2C(C2(CC1=O)C)CCC(=O)C)C	

Table IV. Key targets.

Target	Degree value	Betweenness centrality	Closeness centrality
ESR1	15	0.230	0.430
EGFR	15	0.130	0.410
PIK3CA	15	0.060	0.380
PIK3CB	15	0.060	0.367
PTPN11	15	0.050	0.367

ESR1 and EGFR as representative cases, are illustrated in Fig. 6. Notably, ESR1 exhibited powerful interactions with the core components, with binding energies consistently <-7.0 kcal/mol, suggesting high structural stability (18).

Effects of ZTO on ESR1 and EGFR expression levels in A549 lung cancer cells. To determine whether ZTO exerts its effects through ESR1 and EGFR, RT-qPCR and western blotting analyses were performed to assess changes in the expression levels of these two genes following ZTO treatment. The results demonstrated that, compared with the control group, ZTO significantly downregulated ESR1 and EGFR mRNA levels by 46.56 and 32.61%, respectively (Fig. 7A). At the protein level, ESR1 and EGFR expression decreased by 35.77 and 28.99%, respectively (Fig. 7B). These findings suggested that ZTO inhibited proliferation and induces apoptosis in A549 lung cancer cells by downregulating ESR1 and EGFR expression.

Discussion

A continuous rise in newly diagnosed lung cancer cases in China has been observed in recent years, posing a marked threat to human health (19). The poor prognosis of patients with locally advanced NSCLC may be attributed to the toxic side effects of conventional chemotherapeutic agents on normal cells while targeting tumor cells (20). Traditional Chinese medicine preparations, characterized by multi-target effects and fewer adverse reactions, hold unique advantages. ZTO, primarily composed of volatile oils extracted from *Curcuma zedoaria*, is a natural product containing a number of bioactive components. Clinical and experimental studies have demonstrated its antimicrobial (21), anti-inflammatory (22) and anticancer (23) properties. In the present study, ZTO treatment

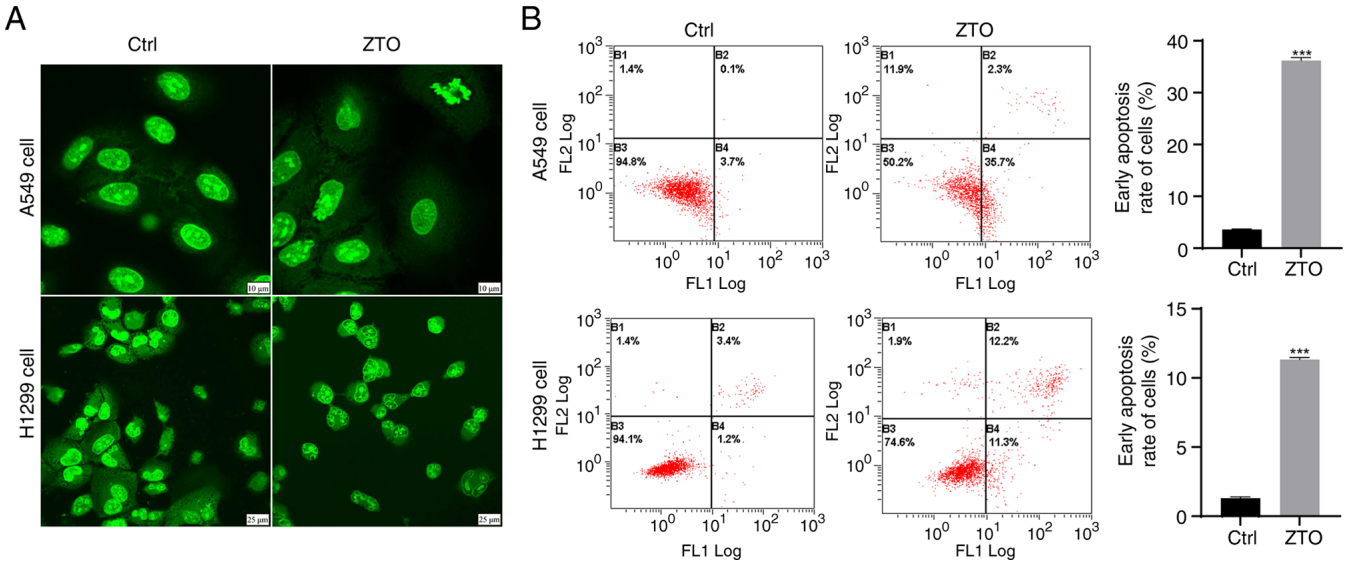

Figure 3. ZTO induces apoptosis in human lung cancer cells. (A) Effect of ZTO on the morphology of human lung cancer A549 cells and H1299 cells. Scale bar, 10 μm (original magnification, x1,000) and 25 μm (original magnification, x400). (B) Effect of ZTO on apoptosis in human lung cancer A549 cells and H1299 cells. ZTO, zedoary turmeric oil; Ctrl, control. ***P<0.001 compared with the control group.

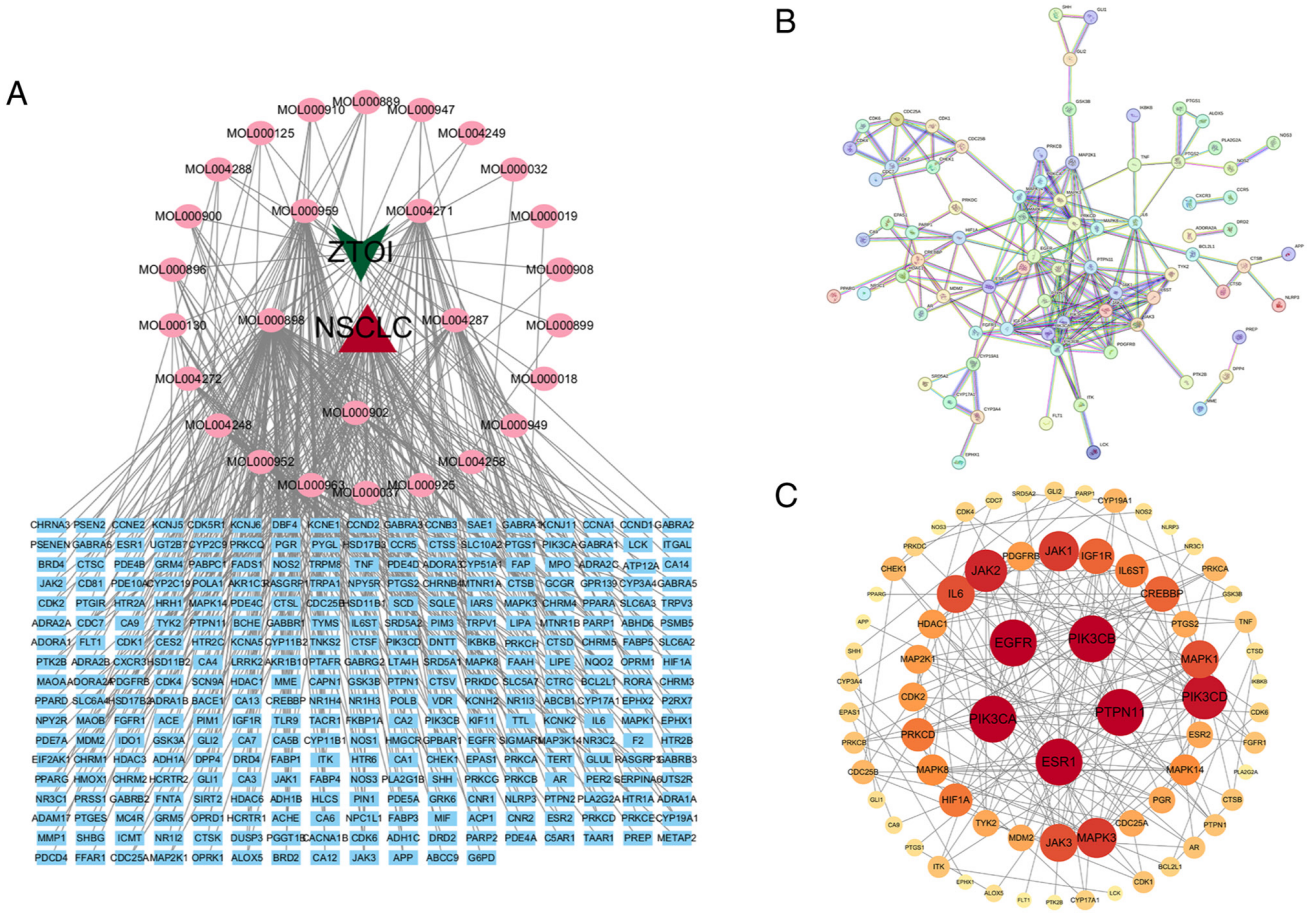

Figure 4. Network pharmacology analysis of intersection targets between ZTO and NSCLC. (A) ZTO-NSCLC-compound-target network diagram. (B) Interaction association of intersection targets between ZTO and NSCLC. (C) Protein-protein interaction network diagram of intersection targets between ZTO and NSCLC. ZTO, zedoary turmeric oil; NSCLC, non-small cell lung cancer.

significantly reduced the viability, colony-forming ability and number of EdU-positive A549 and H1299 cells, as well as inhibited cell migration and increased the early apoptosis rate. These findings indicated that ZTO inhibited proliferation and induced apoptosis in A549 and H1299 human lung cancer cells.

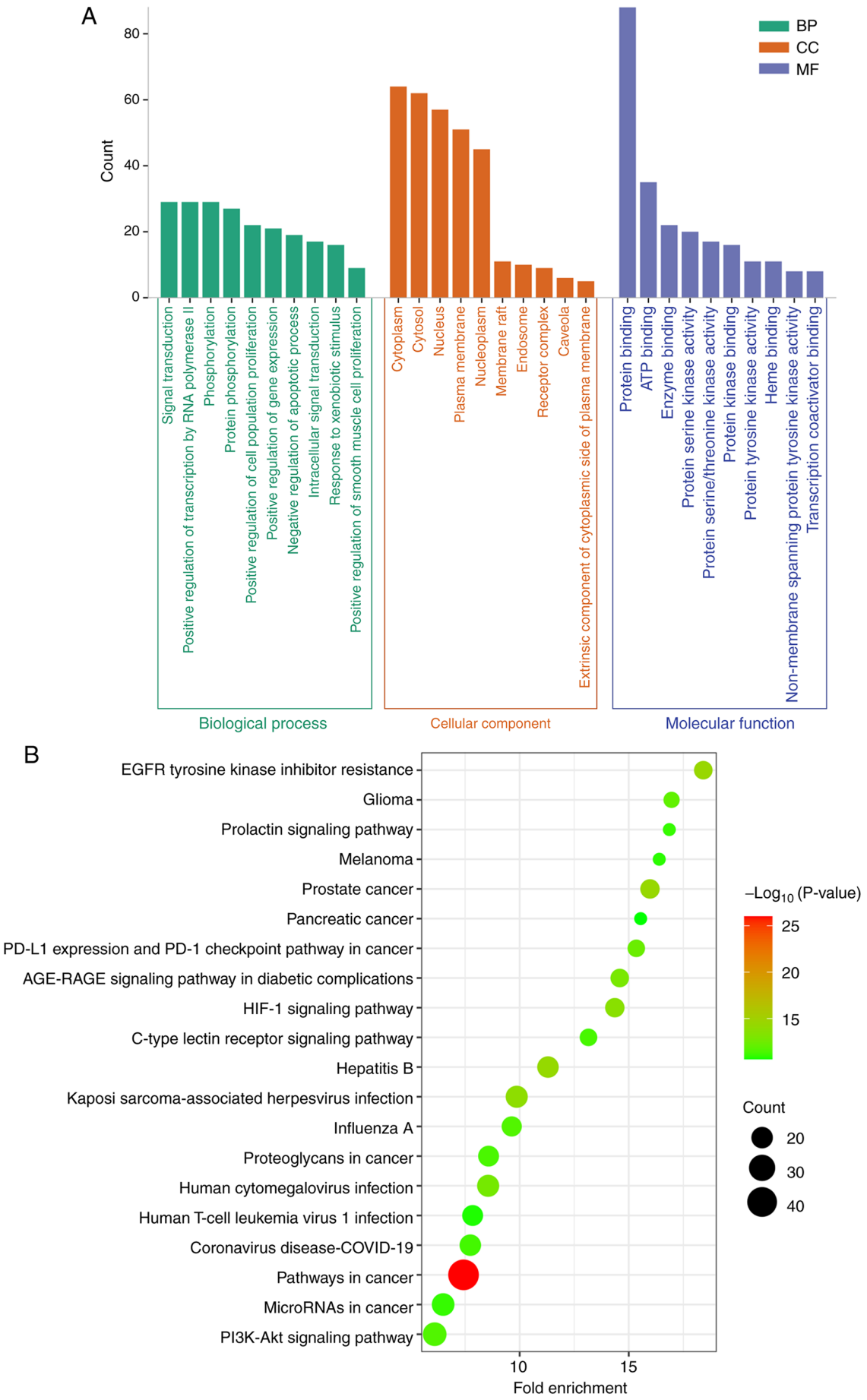

Figure 5. (A) Gene Ontology and (B) Kyoto Encyclopedia of Genes and Genomes pathway enrichment analysis of intersection targets of zedoary turmeric oil and non-small cell lung cancer. BP, biological process; CC, cellular component; MF, molecular function.

Table V. Molecular docking results (kcal/mol).

Compound	Curcumenone	Zedoarondiol	13-Hydroxygermacrone	Neocurdione	Curcumol
ESR1	-7.9	-8.5	-7.8	-7.8	-7.4
EGFR	-6.2	-6.4	-6.3	-6.5	-6.6
PIK3CA	-6.8	-7.8	-7.3	-7.2	-7.7
PIK3CB	-6.7	-7.0	-7.0	-7.5	-6.5
PIPN11	-6.2	-6.5	-6.5	-6.2	-6.4

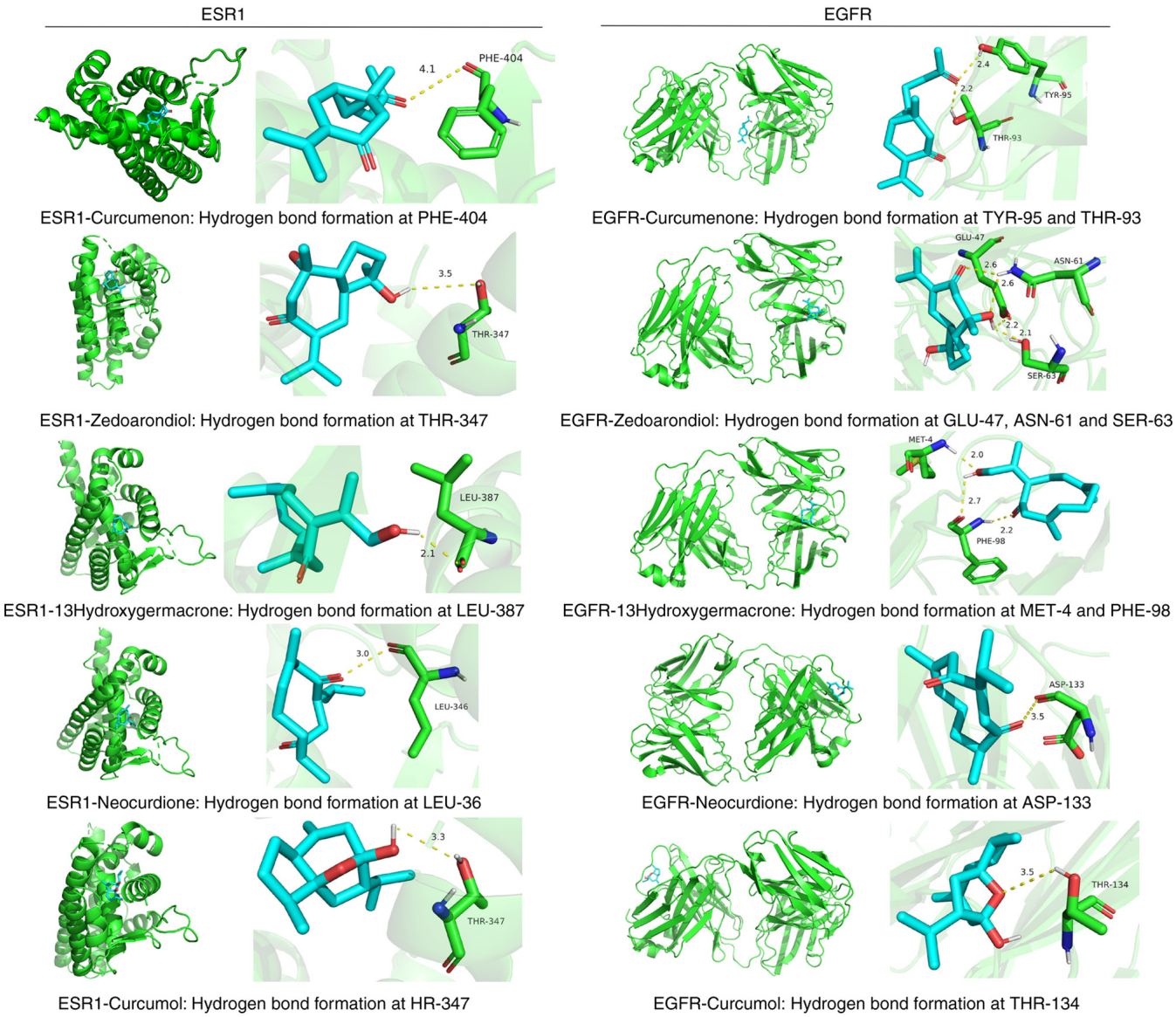

Figure 6. Molecular docking of active ingredients and key targets of zedoary turmeric oil.

However, the chemical composition of ZTO is complex. To clarify the pharmacologically active components responsible for its therapeutic effects, network pharmacology analysis was performed to identify the primary bioactive constituents of ZTO, with results showing that these included curcumenone, zedoarondiol, 13-hydroxygermacrone, neocurdione and curcumol, exhibit extensive potential targets, consistent with findings reported in prior studies (24-30). Curcumol has been identified as an effective inducer of apoptosis in a number of cancer cell types by targeting key signaling pathways commonly dysregulated in malignancies, such as the MAPK/ERK, PI3K/Akt and NF-κB pathways (24-26). Zedoarondiol suppresses the proliferation of human bronchial smooth muscle cells (27), where germacrone inhibited A549

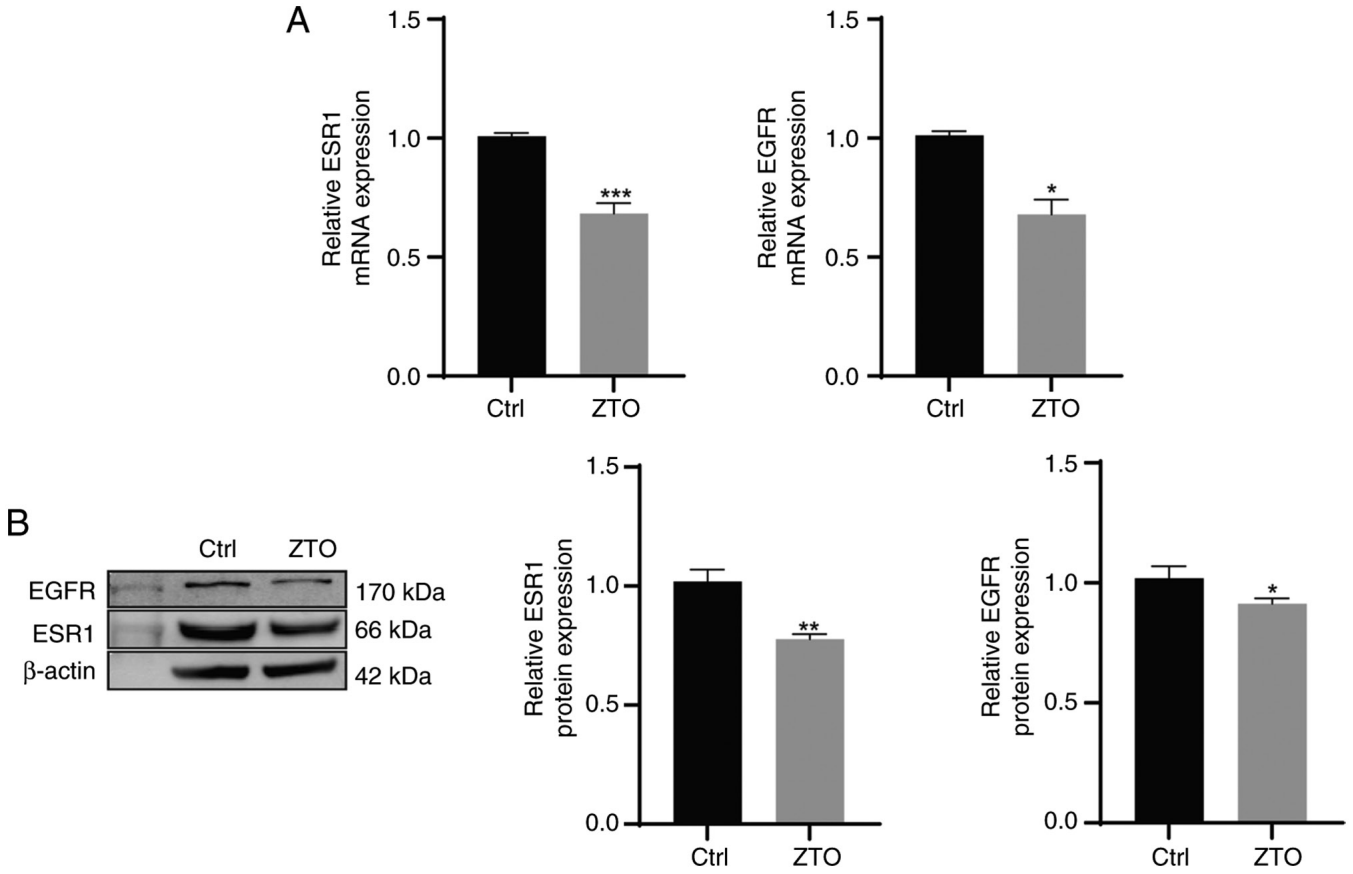

Figure 7. Effects of ZTO on the expression levels of ESR1 and EGFR in human lung cancer A549 cells. (A) Effect of ZTO on ESR1 and EGFR mRNA expression in lung cancer A549 cells. (B) Effect of ZTO on ESR1 and EGFR protein expression in lung cancer A549 cells. *P<0.05 and **P<0.01 compared with the control group. ZTO, zedoary turmeric oil; Ctrl, control.

cell proliferation and induced apoptosis (28). Curcumenone and its associated bioactive components regulate vascular contraction and inflammatory responses (29). Neocurdione has also demonstrated notable tumor growth inhibitory activity (30), collectively indicating that these components likely represent the central constituents underlying the efficacy of ZTO against NSCLC.

GO and KEGG analyses were performed to elucidate the biological processes and signaling pathways underlying the inhibitory effects of ZTO on proliferation and induction of apoptosis in human lung cancer A549 cells. The results revealed that ZTO exerted antitumor effects by modulating the EGFR pathway, PI3K-Akt signaling pathway and other key pathways.

Studies have indicated that EGFR-mediated signaling pathways serve an important role in regulating physiological processes, including cell proliferation and differentiation (31,32). The MAPK and PI3K/Akt pathways, downstream of EGFR, serve a key role in these effects. The PI3K/Akt pathway regulates diverse cellular processes and is critically involved in cancer progression (33). In combination with celecoxib, curcumol has been shown to markedly reduce the phosphorylation of PI3K, Akt, ERK and p38MAPK of A549 and H1299 cells, thereby inducing apoptosis. Notably, the mitogenic PI3K pathway and its downstream NF-κB signaling are known for their ability to suppress apoptosis and promote proliferation (34). Curcumol may also inhibit proliferation and invasion while promoting apoptosis in lung cancer cells by activating the JAK1/STAT3 signaling pathway (35). Zedoarondiol suppresses human bronchial smooth muscle cell proliferation through the caveolin-1/platelet-derived growth factor signaling pathway, potentially by inhibiting the activation of the MAPK and PI3K/AKT pathways (27). Germacrone likely inhibits cell proliferation by modulating the Akt/mouse double minute 2 homolog/p53 signaling axis (28).

PPI network analysis was conducted to identify the core targets underlying the inhibitory effects of ZTO on the proliferation and induction of apoptosis in human lung cancer A549 cells. The PPI network revealed that ESR1, EGFR, PIK3CA, PIK3CB and PTPN11 were the core therapeutic targets of ZTO in NSCLC. ESR1, a key target in the estrogen signaling pathway, has been shown to suppress A549 cell proliferation, migration and xenograft tumor formation in nude mice when knocked down (36). Notably, PIK3CA expression has been associated with EGFR mutations, whereas positive expression of PIK3CB and mTOR increases the risk of lymph node metastasis in patients with lung adenocarcinoma (37). EGFR, a transmembrane protein with cytoplasmic kinase activity, transduces growth factor signals and is a primary therapeutic target in NSCLC. Although EGFR tyrosine kinase inhibitors have been clinically developed to effectively treat NSCLC, drug resistance remains a challenge (38). RT-qPCR and western blotting results demonstrated that ZTO significantly downregulated the mRNA and protein expression of EGFR and ESR1

in A549 cells, leading to reduced proliferative capacity. These findings suggested that ZTO may provide a novel opportunity for synergistic antitumor activity in combination with targeted therapies for NSCLC. Although the present study demonstrated that ZTO downregulated EGFR and ESR1, which are upstream regulators of the PI3K/Akt pathway, whether each core monomeric component individually contributes to this effect and whether there exist synergistic or antagonistic interactions among these components, remains to be elucidated. Furthermore, the present study lacks *in vivo* animal experimental data. The antitumor activity, bioavailability and systemic toxicity of ZTO and its monomeric components in animal models of non-small cell lung cancer therefore await further validation.

In summary, the present study employed network pharmacology to identify potential core components and key targets of ZTO in the treatment of NSCLC. Molecular docking analysis revealed favorable binding interactions between these core components and their targets, indicating their robust pharmacological activity. *In vitro* experiments determined that ZTO inhibits the proliferation of A549 cells and downregulates the expression of ESR1 and EGFR, which are pivotal regulators of oncogenic signaling pathways. These findings indicated that ZTO exerts its therapeutic effects on NSCLC through a complex network mechanism involving multicomponent synergy, multi-target modulation and multi-pathway regulation. Further in-depth investigations should be pursued in subsequent studies. The present study therefore provides marked theoretical support for the clinical translation of ZTO and highlights its potential as a complementary agent in targeted NSCLC therapies.

Acknowledgements

Not applicable.

Funding

The present study was supported by the Natural Science Foundation of Heilongjiang Province (grant no. LH2023H104) and the Traditional Chinese Medicine Scientific Research Project of Heilongjiang Province (grant no. ZHY2025-299).

Availability of data and materials

The data generated in the present study are included in the figures and/or tables of this article.

Authors' contributions

HL and WZ conceptualized the present study. QY performed the confocal laser microscope imaging and analysis. HL, LL, YL and YS performed the bioinformatics analyses, including molecular docking and network pharmacology analysis. JJ, ZW, WZ and BL performed data analysis. HL, LL and WZ wrote, reviewed and edited the original manuscript. HL provided supervision and acquired funding for the present study. HL and BL confirm the authenticity of all the raw data. All authors read and approved the final manuscript.

Ethics approval and consent to participate

Not applicable.

Patient consent for publication

Not applicable.

Competing interests

The authors declare that they have no competing interests.

References

1. Bray F, Laversanne M, Sung H, Ferlay J, Siegel RL, Soerjomataram I and Jemal A: Global cancer statistics 2022: GLOBOCAN estimates of incidence and mortality worldwide for 36 cancers in 185 countries. CA Cancer J Clin 74: 229-263, 2024.
2. Chen P, Liu Y, Wen Y and Zhou C: Non-small cell lung cancer in China. Cancer Commun (Lond) 42: 937-970, 2022.
3. Herbst RS, Morgensztern D and Boshoff C: The biology and management of non-small cell lung cancer. Nature 553: 446-454, 2018.
4. Siegel RL, Kratzer TB, Wagle NS, Sung H and Jemal A: Cancer statistics, 2026. CA Cancer J Clin 76: 70043, 2026.
5. Chinese Pharmacopoeia Commission. Pharmacopoeia of the People's Republic of China 2020 Edition. Vol I. China Medical Science Press, Beijing, pp479, 2020. (Standard No.: Zedoary Turmeric Oil).
6. Cui T, Li BY, Liu F and Xiong L: Research progress on sesquiterpenoids of curcumae rhizoma and their pharmacological effects. Biomolecules 14: 387, 2024.
7. Zhong M, Li Y, Wang H, Fan N, Chu X, Liu L, Zhao C, Sun Y, Zhang S and Fu H: Integrated network pharmacology and experimental validation reveal EGFR/p53/Bcl-2-mediated anti-hepatocellular carcinoma effects of Zedoary Turmeric Oil. J Ethnopharmacol 352: 120241, 2025.
8. Zhou JL, Zheng JY, Cheng XQ, Xin GZ, Wang SL and Xie T: Chemical markers' knockout coupled with UHPLC-HRMS-based metabolomics reveals anti-cancer integration effects of the curcuminoids of turmeric (*Curcuma longa* L.) on lung cancer cell line. J Pharm Biomed Anal 175: 112738, 2019.
9. Cho HK, Park CG and Lim HB: Construction of a synergy combination model for turmeric (*Curcuma longa* L.) and black pepper (*Piper nigrum* L.) Extracts: Enhanced anticancer activity against A549 and NCI-H292 human lung cancer cells. Curr Issues Mol Biol 46: 5551-5560, 2024.
10. Ashrafizadeh M, Najafi M, Makvandi P, Zarrabi A, Farkhondeh T and Samarghandian S: Versatile role of curcumin and its derivatives in lung cancer therapy. J Cell Physiol 235: 9241-9268, 2020.
11. Wu YZ, Zhang Q, Wei XH, Jiang CX, Li XK, Shang HC and Lin S: Multiple anti-inflammatory mechanisms of Zedoary turmeric oil Injection against lipopolysaccharides-induced acute lung injury in rats elucidated by network pharmacology combined with transcriptomics. Phytomedicine 106: 154418, 2022.
12. Yang Z, Wang Z, Li J, Long J, Peng C and Yan D: Network pharmacology-based dissection of the underlying mechanisms of dyspnoea induced by Zedoary turmeric oil. Basic Clin Pharmacol Toxicol 130: 606-617, 2022.
13. Tong H, Yu M, Fei C, Ji D, Dong J, Su L, Gu W, Mao C, Li L, Bian Z, *et al*: Bioactive constituents and the molecular mechanism of *Curcumae Rhizoma* in the treatment of primary dysmenorrhea based on network pharmacology and molecular docking. Phytomedicine 86: 153558, 2021.
14. Zhang P, Zhang D, Zhou W, Wang L, Wang B, Zhang T and Li S: Network pharmacology: Towards the artificial intelligence-based precision traditional Chinese medicine. Brief Bioinform 25: bbad518, 2023.
15. Shannon P, Markiel A, Ozier O, Baliga NS, Wang JT, Ramage D, Amin N, Schwikowski B and Ideker T: Cytoscape: A software environment for integrated models of biomolecular interaction networks. Genome Res 13: 2498-2504, 2003.
16. Zhang W, Tong H, Zhang Z, Shao S, Liu D, Li S and Yan Y: Transcription factor EGR1 promotes differentiation of bovine skeletal muscle satellite cells by regulating MyoG gene expression. J Cell Physiol 233: 350-362, 2018.

17. Livak KJ and Schmittgen TD: Analysis of relative gene expression data using real-time quantitative PCR and the 2(-Delta Delta C(T)) method. Methods 25: 402-408, 2001.
18. Wang Z, Wang X, Guo Z, Liao H, Chai Y, Wang Z and Wang Z: Reduning attenuates LPS-Induced human unmilical vein endothelial cells (HUVECs) apoptosis through PI3K-AKT signaling pathway. Front Pharmacol 13: 921337, 2022.
19. Siegel RL, Miller KD, Fuchs HE and Jemal A: Cancer statistics, 2022. CA Cancer J Clin 72: 7-33, 2022.
20. Jeon H, Wang S, Song J, Gill H and Cheng H: Update 2025: Management of Non-Small-cell lung cancer. Lung 203: 53, 2025.
21. Li L, Xie Q, Bian G, Zhang B, Wang M, Wang Y, Chen Z and Li Y: Anti-H1N1 viral activity of three main active ingredients from zedoary oil. Fitoterapia 142: 104489, 2020.
22. Wu YZ, Zhang Q, Li H, Jiang CX, Li XK, Shang HC and Lin S: Zedoary turmeric oil injection ameliorates lung inflammation via platelet factor 4 and regulates gut microbiota disorder in respiratory syncytial virus-infected young mice. Chin Med 19: 83, 2024.
23. Zhu G, Shen Q, Jiang H, Ji O, Zhu L and Zhang L: Curcumin inhibited the growth and invasion of human monocytic leukaemia SHI-1 cells in vivo by altering MAPK and MMP signalling. Pharm Biol 58: 25-34, 2020.
24. Wei W, Rasul A, Sadiqa A, Sarfraz I, Hussain G, Nageen B, Liu X, Watanabe N, Selamoglu Z, Ali M, *et al*: Curcumol: From plant roots to cancer roots. Int J Biol Sci 15: 1600-1609, 2019.
25. Ning N, Liu S, Liu X, Tian Z, Jiang Y, Yu N, Tan B, Feng H, Feng X and Zou L: Curcumol inhibits the proliferation and metastasis of melanoma via the miR-152-3p/PI3K/AKT and ERK/NF-κB signaling pathways. J Cancer 11: 1679-1692, 2020.
26. Huang X, Qian J, Li L, Zhang X, Wei G, Lv J, Qin F, Yu J, Xiao Y, Gong Z and Huo J: Curcumol improves cisplatin sensitivity of human gastric cancer cells through inhibiting PI3K/AKT pathway. Drug Dev Res 81: 1019-1025, 2020.
27. Lyu Y, Feng W, Song J, Wang C, Fu Y, Zhao B and Meng Y: Zedoarondiol inhibits human bronchial smooth muscle cell proliferation through the CAV-1/PDGF signalling pathway. Sci Rep 14: 13145, 2024.
28. Zhao Y, Cai J, Shi K, Li H, Du J, Hu D, Liu Z and Wang W: Germacrone induces lung cancer cell apoptosis and cell cycle arrest via the Akt/MDM2/p53 signaling pathway. Mol Med Rep 23: 452, 2021.
29. Xie H, Su D, Zhang J, Ji D, Mao J, Hao M, Wang Q, Yu M, Mao C and Lu T: Raw and vinegar processed *Curcuma wenyujin* regulates hepatic fibrosis via bloking TGF-β/Smad signaling pathways and up-regulation of MMP-2/TIMP-1 ratio. J Ethnopharmacol 246: 111768, 2020.
30. Syed Abdul Rahman SN, Abdul Wahab N and Abd Malek SN: In vitro morphological assessment of apoptosis induced by antiproliferative constituents from the rhizomes of curcuma zedoaria. Evid Based Complement Alternat Med 2013: 257108, 2013.
31. Ye L, Chen X and Zhou F: EGFR-mutant NSCLC: Emerging novel drugs. Curr Opin Oncol 33: 87-94, 2021.
32. Stella GM, Luisetti M, Inghilleri S, Cemmi F, Scabini R, Zorzetto M and Pozzi E: Targeting EGFR in non-small-cell lung cancer: Lessons, experiences, strategies. Respir Med 106: 173-183, 2012.
33. Faes S and Dormond O: PI3K and AKT: Unfaithful partners in cancer. Int J Mol Sci 16: 21138-21152, 2015.
34. Cai F, Chen M, Zha D, Zhang P, Zhang X, Cao N, Wang J, He Y, Fan X, Zhang W, *et al*: Curcumol potentiates celecoxib-induced growth inhibition and apoptosis in human non-small cell lung cancer. Oncotarget 8: 115526-115545, 2017.
35. Shien K, Papadimitrakopoulou VA, Ruder D, Behrens C, Shen L, Kalhor N, Song J, Lee JJ, Wang J, Tang X, *et al*: JAK1/STAT3 activation through a proinflammatory cytokine pathway leads to resistance to molecularly targeted therapy in Non-Small cell lung cancer. Mol Cancer Ther 16: 2234-2245, 2017.
36. Liu Y, Ma H and Yao J: ERα, A key target for cancer therapy: A review. Onco Targets Ther 13: 2183-2191, 2020.
37. Song Z, Yu X and Zhang Y: Mutation and prognostic analyses of PIK3CA in patients with completely resected lung adenocarcinoma. Cancer Med 5: 2694-2700, 2016.
38. Dong RF, Zhu ML, Liu MM, Xu YT, Yuan LL, Bian J, Xia YZ and Kong LY: EGFR mutation mediates resistance to EGFR tyrosine kinase inhibitors in NSCLC: From molecular mechanisms to clinical research. Pharmacol Res 167: 105583, 2021.